PERGAMON

International Journal of Solids and Structures 39 (2002) 4867–4887

INTERNATIONAL JOURNAL OF SOLIDS and STRUCTURES

www.elsevier.com/locate/ijsolstr

Thermo-elastic buckling of layered shell segments

S.E. Rutgerson [1], W.J. Bottega *

Department of Mechanical and Aerospace Engineering, Rutgers University, 98 Brett Road, Piscataway, NJ 08854-8058, USA

Received 20 February 2002

Abstract

The buckling behavior of multilayer shells is studied for composite structures subjected to combinations of uniform temperature change, applied external pressure, and applied and reactive circumferential edge loads. A stability criterion is established for the class of structures of interest and a transverse loading parameter is identified. Critical parameters are identified, and closed form analytical solutions are obtained for the associated non-linear problems. Numerical simulations, based on these solutions, are performed and the stability criterion is applied, revealing characteristic behavior of the structures of interest. Such behavior includes "sling-shot" buckling, whereby the structure slings from deflections in one direction to deflections in the opposite sense, in an unstable manner, at critical temperatures. The influence of external pressure on the critical temperature change of thermally loaded composite structures is elucidated, as is the influence of temperature change on the buckling behavior of pressure loaded multilayer shells.

Keywords: Thermo-elastic; Buckling; Shells; Layer; Composite; Laminate; Sling-shot buckling; Snap-through

1. Introduction

Layered structures can be found in an extensive array of applications ranging from laminated structures in aircraft to thin film deposition in semiconductor devices. Such structures are subjected to a variety of loading types and often to severe temperature changes. As the layers comprising such structures generally possess disparate thermal expansion coefficients, such temperature changes can introduce additional stresses and moments which often lead to interesting and unexpected behavior.

Studies pertaining to thermally induced buckling of layered structures have been reported in the literature and include the classic papers of Timoshenko (1925), Wahl (1944), Wittrick (1953) and Wittrick et al. (1953). The former two studies were concerned with the response of bilayer strips while the latter two were concerned with the response of a shallow bilayer spherical cap modeled as a circular plate with initial deflection. Critical temperatures were assumed to correspond to limit points of a temperature-deflection

* Corresponding author. Tel.: +1-732-445-4282; fax: +1-732-445-5313.
E-mail address: bottega@rci.rutgers.edu (W.J. Bottega).
[1] Present address: Naval Surface Warfare Center, Carderock Div., West Bethesda, MD 20817-5700, USA.

0020-7683/02/$ - see front matter
PII: S0020-7683(02)00415-8

curve, and classic snap-through was assumed to follow. Likewise, Chen and Chen (1990) and Noor and Burton (1992) studied thermal buckling of composite cylinders subjected to non-uniform temperature fields and predicted snap-through buckling at critical temperatures. Huang and Tauchert (1991) studied buckling of cylindrical shells due to uniform thermal loading, via finite element analysis. Other related studies include Boley and Weiner (1960), Brevik and Hyer (1998), Gauss and Antman (1984), Hamamoto and Hyer (1987), Huang and Tauchert (1988), Librescu and Souza (1993), Mahayni (1966), Muller de Almeida and Hansen (1997), Noor and Peters (1992a,b), Noor et al. (1993), Tauchert (1991) and Yin (1998). A more detailed discussion can be found in (Karlsson and Bottega, 2000a).

Recent work of Rutgerson and Bottega (submitted for publication) concerning buckling of layered shell segments subjected to external pressure includes a formal stability analysis of the equilibrium configurations of the deforming structure and shows that snap-through buckling occurs below, and often well below, the limit load of the load-deflection curve. Critical behavior was seen to be associated with the crossing of branches of the roots of an integrability condition associated with the circumferential displacements. Recent work of Karlsson and Bottega (2000a,b,c) pertaining to thermal buckling of patched plates demonstrated "sling-shot buckling", whereby the sense of the deformation switches and slings in an unstable manner at a critical temperature not associated with a limit point. The present work expands on these concepts, and those introduced by Rutgerson (2001), and Bottega and Rutgerson (2001), to examine the buckling behavior of multilayer shell segments subjected to uniform temperature, and a combination of uniform temperature and external pressure, as well as both reactive and active circumferential edge loads. In doing so, the phenomena of "sling-shot buckling" and "pre-limit point snap-through" will be further elucidated as will the understanding of the behavior of composite shell segments under the load types considered.

In the present study, we consider the thermo-elastic behavior of shallow multilayer shell segments in plane strain and plane stress configurations where each of the layers may possess different material, thicknesses and thermal properties. The problem is expressed in a mixed formulation in terms of the transverse (radial) displacements and the resultant membrane force of the composite structure. A loading parameter is identified consisting of a combination of the normalized pressure and thermal moment. A stability criterion, based on the second variation of the total potential energy of the system is derived in terms of small perturbations away from equilibrium configurations of interest, for situations where multiple equilibrium configurations are possible for a given value of the loading parameter. Closed form analytical solutions are obtained for the associated non-linear problem, and the corresponding membrane force is evaluated numerically as roots of a transcendental equation resulting from an integrability condition associated with the circumferential displacements. Extensive results of numerical simulations based on the aforementioned analytical solutions are presented and characteristic behavior is revealed for the cases of clamped-free, pinned-free, clamped-fixed and pinned-fixed support conditions. For the former two support types, where the edges of the structure are free to translate in the circumferential direction, we consider the structure to be subjected to an applied circumferential edge load together with external pressure and uniform temperature change. For the latter two cases, where the structure is fixed with regard to circumferential translation, we consider two loading scenarios: (i) where the structure is subjected to a uniform temperature change alone, and (ii) where the structure is subjected to both a uniform pressure over its external convex surface and to uniform temperature changes. It is seen that the overall behavior and, in particular, the buckling of the composite shell is influenced by a ratio of two of the composite mechanical stiffnesses and to a ratio of composite thermal stiffness properties, and that the behavior is characterized by a critical value of the normalized loading parameter and by a critical value of the normalized membrane force, the latter of which is seen to be independent of the particular material properties of the system. Bifurcation buckling, asymptotic buckling and sling-shot buckling are all seen to occur under appropriate circumstances. It is also seen that pre-limit buckling exhibited for pressure loaded structures in (Rutgerson and Bottega, submitted for publication) is further enhanced by the effects of temperature.

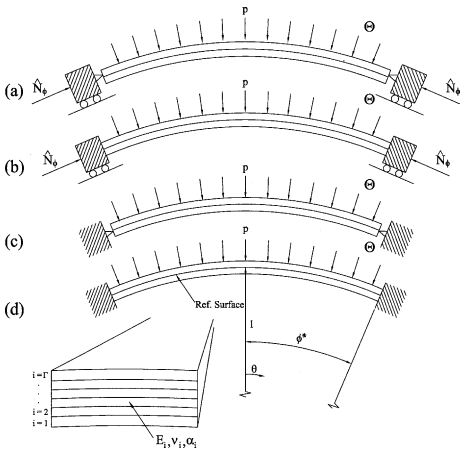

Fig. 1. Multilayer shell structure subjected to applied pressure, temperature change, and circumferential edge load: (a) pinned-free supports, (b) clamped-free supports, (c) pinned-fixed supports, (d) clamped-fixed supports.

2. Problem statement

Consider a shell structure comprised of multiple cylindrical layers, numbered 1 through Γ, which are bonded over their common interfaces. Each layer is characterized by its normalized (see Appendices A and C) Young's modulus and coefficient of thermal expansion, E_i and α_i respectively, the associated Poisson's ratio, ν_i, and the corresponding normalized thickness, $h_i \ll 1$ $(i = 1, 2, \ldots, \Gamma)$. In what follows, all length scales are normalized with respect to the undeformed radius of the "reference surface". This surface may be taken, for example, as the geometric center of the cross section, the neutral surface, or a convenient interface. In this context, the structure is described by the angular coordinate θ, measured clockwise from the center of the span, and the structure is defined over the region $-\phi^* \leqslant \theta \leqslant \phi^*$, as indicated in Fig. 1. The structure is subjected to a uniform normalized radial pressure, $\hat{p}$ (see Appendix D), acting on the convex surface of the outermost layer $(i = \Gamma)$, and to a uniform normalized temperature change, $\widetilde{\Theta}$, which manifests itself as a normalized distributed thermal moment, $\widehat{\Theta}$. The natural temperature scale and corresponding normalization may be found in Appendix A. The kinematic relations which define the composite shell as an assemblage of Γ shallow shells, and the governing equations and boundary conditions, as well as the constitutive relations of the composite structure, are obtained by paralleling the variational development of Bottega (1994) [2] and Bottega and Karlsson (1999), and incorporating the thermally induced strains as in (Karlsson and Bottega, 2000a). The pertinent kinematic relations are given in Appendix B, the constitutive relations obtained for the composite structure are given in Appendix C, and the resulting governing equations for the mixed formulation are given by

$$w'''' + (2 + \widehat{N})w'' + w = \hat{p} + \widehat{\Theta} - (1 - \rho^*)\widehat{N}, \tag{1a}$$

$$\widehat{N}' = 0, \tag{1b}$$

[2] For the present study, the intact region of (Bottega, 1994), or the intact patched region of (Bottega and Karlsson, 1999) is taken to envelop the entire structure.

where superposed primes indicate total differentiation with respect to θ, $w(\theta)$ is the normalized radial deflection (positive inward), and $\widehat{N}$ is the normalized (compressive) membrane force as defined in Appendix D. The non-dimensional parameter ρ^* ($\ll 1$) is a material property (see Appendix C) and locates the centroid of the composite structure with respect to the reference surface. In addition, $u^*(\theta)$ represents the circumferential displacement at the reference surface (positive in the direction of increasing θ) and $\hat{u}(\theta)$ represents the analogous displacement at the neutral surface of the composite structure. The two are related through Eq. (B.2). Further, for cases for which the edges of the structure are free to translate circumferentially (clamped-free or pinned-free supports), we consider the structure to be loaded by the normalized (compressive) circumferential edge load, $\widehat{N}_\phi$, as well.

The associated boundary conditions corresponding to symmetric solutions with respect to θ are given by

$$\hat{u}(0) = 0, \qquad w'(0) = 0, \qquad \left[w''' + (1 + \widehat{N})w'\right]_{\theta=0} = 0, \tag{2a–c}$$

$$w(\phi^*) = 0, \tag{3a}$$

and, depending on the type of supports,

$$\hat{u}(\phi^*) = 0 \quad \text{(edges fixed with regard to circumferential translation)} \tag{3b$_1$}$$

or

$$\widehat{N}(\phi^*) = \widehat{N}_\phi \quad (\widehat{N}_\phi \text{ prescribed, edges free to translate circumferentially}), \tag{3b$_2$}$$

and either

$$w'(\phi^*) = 0 \quad \text{(clamped supports)} \quad \text{or} \quad \left[w'' + w\right]_{\theta=\phi^*} = 0 \quad \text{(pinned supports)}. \tag{3c$_1$, c$_2$}$$

Integration of the constitutive relation (C.1a) over $[0, \phi^*]$ gives the integrability condition

$$\hat{u}(\phi^*) - \hat{u}(0) = \frac{\phi^*}{C^*/D^*}\left[\frac{n^*}{m^*}\widehat{\Theta} - \widehat{N}\right] + (1 - \rho^*)\int_0^{\phi^*} w\,\mathrm{d}\theta - \frac{1}{2}\int_0^{\phi^*} w'^2\,\mathrm{d}\theta. \tag{4}$$

In the above expressions, C^* and D^* are mechanical stiffnesses of the composite structure, ρ^* is a ratio of composite stiffnesses and locates the mechanical centroid of the cross section with respect to the reference surface, the parameter n^* is a membrane force per unit temperature change of the composite structure and m^* is a bending moment per unit temperature change (see Appendix C).

3. Stability criterion

When the supports are such that circumferential translation at the edges of the structure are prohibited (clamped-fixed and pinned-fixed supports), multiple equilibrium configurations are generally possible for a given value of the loading parameter, $\hat{\lambda}$. In such situations, we must determine which of the possible configurations the structure will tend toward (i.e., which configuration is stable). We shall accomplish this by introducing small perturbations to the deformation corresponding to a given equilibrium configuration, and then examining the second variation of the total potential energy of the system, as in (Bottega and Rutgerson, 2001; Rutgerson and Bottega, submitted for publication). If the second variation of the total potential energy for a given configuration is positive definite, the equilibrium configuration will be said to be stable. If it is not, the equilibrium configuration will be considered unstable. Toward this end, we shall perturb the transverse displacement, w, and hence the curvature change κ (as given by Eq. (B.1b)), and also the membrane strain e^*.

It may be anticipated that the solutions to Eqs. (1a,b), for the radial deflection corresponding to a given equilibrium configuration, will be of the general form

$$w(\theta) = \widehat{Q} W(\theta, \widehat{N}_{\mathrm{eq}}), \tag{5}$$

where $\widehat{N}_{\mathrm{eq}}$ represents the particular value of the membrane force at the equilibrium configuration in question. The perturbation of the transverse displacement will thus be implemented by perturbing the amplitude $\widehat{Q}$. The perturbation of the membrane strain is accomplished by incorporating the perturbation of the radial displacement into Eq. (C.1a) and perturbing the (reactive) membrane force. (Recall that, in this section, we are considering situations where the edges of the structure are fixed with regard to circumferential translation.) Thus, for the present formulation, the perturbation of the membrane strain is introduced through an equivalent perturbation of the membrane force. Expanding the transverse displacement and the membrane force about their respective equilibrium values, w_{eq} and $\widehat{N}_{\mathrm{eq}}$, we have

$$w = w_{\mathrm{eq}} + W\delta\widehat{Q} \quad \text{and} \quad \widehat{N} = \widehat{N}_{\mathrm{eq}} + \delta\widehat{N}, \tag{6a, b}$$

where $\delta\widehat{Q}$ and $\delta\widehat{N}$ are arbitrary. Substitution of the expressions (6a,b) into the total potential energy, Π, and retaining terms of second order gives the second variation of the total potential energy, $\delta^2\Pi$, in the form

$$\delta^2\Pi = \frac{\phi^*}{2C^*}(\delta\widehat{N})^2 + \widehat{N}_{\mathrm{eq}} F^* (\delta\widehat{Q})^2. \tag{7}$$

The parameter F^*, appearing in Eq. (7), will be referred to as the "stability function" and is given by

$$F^* = F^*(\widehat{N}_{\mathrm{eq}}) \equiv \int_0^{\phi^*} \frac{D^*}{2\widehat{N}_{\mathrm{eq}}} \left[W''(\theta; \widehat{N}_{\mathrm{eq}}) + W(\theta; \widehat{N}_{\mathrm{eq}}) \right]^2 \mathrm{d}\theta - \frac{1}{2} \int_0^{\phi^*} W'^2(\theta; \widehat{N}_{\mathrm{eq}})\, \mathrm{d}\theta. \tag{8}$$

As $\delta\widehat{Q}$ and $\delta\widehat{N}$ are arbitrary and $\widehat{N}_{\mathrm{eq}} > 0$, it is evident that the right hand side of Eq. (7) will be positive definite if the associated coefficients are positive. This leads to the following stability criterion:

An equilibrium configuration is stable if $F^* > 0$. It is unstable otherwise. (9)

4. Analytical solution

Eqs. (1a,b) together with the boundary conditions (2a–c) and (3a–c) are solved analytically giving solutions of the form

$$w(\theta) = \widehat{Q} W(\theta; \widehat{N}) = \widehat{Q} \left[\frac{G(\theta; \widehat{N})}{F_0(\phi^*; \widehat{N})} + 1 \right], \tag{10}$$

where,

$$\widehat{Q} = \hat{\lambda} - (1 - \rho^*)\widehat{N} \approx \hat{\lambda} - \widehat{N}, \tag{11}$$

and

$$\hat{\lambda} = \hat{p} + \widehat{\Theta}. \tag{12}$$

The parameter $\hat{\lambda}$, which is seen to be comprised of the applied pressure and a thermal moment per unit length, may be identified as the "loading parameter" for the class of problems for which the supports are fixed with regard to circumferential translation and can be viewed as an effective pressure. The specific

forms of the functions G and F_0 appearing in Eq. (10) depend upon the rotational constraints of the supports as follows:

clamped supports:

$$G = G_c \equiv a^2 \sin(a\phi^*)\cos(\theta/a) - \sin(\phi^*/a)\cos(a\theta), \tag{13a}$$

$$F_0 = F_{0c} \equiv \cos(a\phi^*)\sin(\phi^*/a) - \sin(a\phi^*)\cos(\phi^*/a), \tag{13b}$$

pinned supports:

$$G = G_p \equiv \cos(\phi^*/a)\cos(a\theta) - a^4\cos(a\phi^*)\cos(\theta/a), \tag{14a}$$

$$F_0 = F_{0p} \equiv (a^4 - 1)\cos(a\phi^*)\cos(\phi^*/a), \tag{14b}$$

where the parameter a, appearing in Eqs. (13a,b) and (14a,b), is given by

$$a = \sqrt{\frac{(2+\widehat{N}) + \sqrt{\widehat{N}(4+\widehat{N})}}{2}}. \tag{15}$$

In problems for which the edges of the structures are free to translate, the membrane force is prescribed through the boundary condition ($3b_2$) and Eq. (1b). Substitution of the above solution into Eq. (4) then gives the associated circumferential edge deflection, $\hat{u}(\phi^*)$. In problems for which the edges of the structure prohibit circumferential translation, the values of the membrane force corresponding to equilibrium configurations of the composite structure may be found by substituting the appropriate solution described above, by Eqs. (10)–(12) and either (13a,b) or (14a,b), into the integrability condition (4) subjected to the boundary conditions (2a) and ($3b_1$), and solving the resulting transcendental equation numerically for $\widehat{N}$ as a function of $\hat{\lambda}$. Each $(\widehat{N}, \hat{\lambda})$ pair may then be substituted back into Eq. (10), using Eqs. (11)–(15), to obtain the associated radial deflection, $w(\theta)$. As multiple roots, and hence multiple equilibrium configurations, are possible for a given value of the loading parameter for this case, an assessment of the stability of the various equilibrium configurations is warranted. This is accomplished by substituting the displacement functions corresponding to the equilibrium configurations of interest into Eq. (8) and applying the stability criterion (9).

5. Critical parameters

It will be seen that there are two critical parameters, a critical membrane force and a critical loading parameter, that distinguish the behavior of the structures of interest. Upon examination of Eq. (10), it may be seen that the expression for the radial deflection becomes singular when F_0 vanishes, and when $\widehat{Q}$ and F_0 vanish simultaneously. It will be seen that these conditions are associated with critical behavior of the structure. As both F_{0c} and F_{0s} are seen to be functions solely of the membrane force and the half-length, it is seen that the roots of this condition yield critical values of the membrane force for given ϕ^*. Hence,

$$F_0(\widehat{N}; \phi^*) = 0 \Rightarrow \widehat{N}_{cr}, \tag{16}$$

where F_0 is given by Eq. (13b) or (14b) depending upon the support condition, and $\widehat{N}_{cr}$ corresponds to the lowest roots of Eq. (16) and is designated as "the critical membrane force". Likewise, it is seen from Eqs. (11), (12), (13b) and (14b), that simultaneous vanishing of $\widehat{Q}$ and F_0 yield specific values of the loading parameter associated with $\widehat{N}_{cr}$. Such critical values of the loading parameter are designated as $\hat{\lambda}_{cr}$. Hence,

$$F_0 = 0 \text{ and } \widehat{Q} = 0 \Rightarrow \hat{\lambda}_{cr} = (1-\rho^*)\widehat{N}_{cr} \approx \widehat{N}_{cr}. \tag{17}$$

With the exception of the half-length of the span, the critical membrane force is seen to be independent of the material and geometric properties of the structure. This is seen to be, effectively, the case for the "critical loading parameter" as well.

6. Results and discussion

In this section, results are presented for clamped and pinned edge conditions. In each case, three loading scenarios will be examined. In the first scenario, the ends of the structure are free to move circumferentially (clamped-free and pinned-free supports) while the shell is subjected to prescribed circumferential edge loading and given values of the loading parameter. In the second and third loading scenarios, the edges of the structure are fixed so as to prohibit circumferential translation (clamped-fixed and pinned-fixed supports). For the second scenario, we consider pure thermal loading, while for the third we consider the effects of temperature change on pressure loaded shells and vice-versa. For the latter two cases, the membrane force is found numerically, as roots of the explicit form of the integrability condition (4) for given values of the loading parameter. The method employed is a hybrid between an incremental step based root finding method and the bisection technique. Stability is assessed using the criterion of Section 3.

The renormalized critical membrane force, $\widehat{N}_{\mathrm{cr}}$, as defined by Eq. (16), together with the critical loading parameter, $\hat{\lambda}_{\mathrm{cr}}$, is central to critical behavior pertaining to all of the aforementioned loading scenarios. The dependence of the former on the normalized half-span length, ϕ^*, is displayed in Fig. 2(a) and (b) for the cases of clamped supports and pinned supports, respectively.

Before proceeding, we first identify the "characteristic deflections" for the system as the circumferential edge deflection and the transverse centerspan deflection, respectively denoted as

$$U_\phi \equiv \hat{u}(\phi^*) \quad \text{and} \quad w_0 \equiv w(0). \tag{18a, b}$$

6.1. Prescribed circumferential edge loading

In this section we consider the edges of the structure to be free to translate circumferentially, while the structure is subjected to an applied (compressive) circumferential edge load and is simultaneously subjected to an applied pressure and a uniform temperature. We consider both clamped-free and pinned-free supports and present results for the former first.

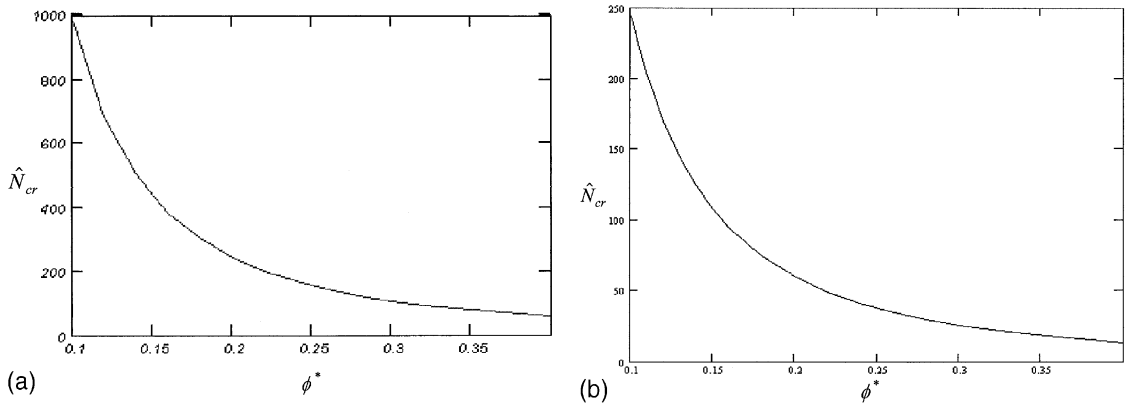

Fig. 2. Critical membrane force parameter as a function of half-span length: (a) clamped supports, (b) pinned supports.

Results for the case of a structure possessing clamped-free supports and subjected to an applied circumferential edge load, are displayed in the form of load-deflection curves in Figs. 3 and 4, for a representative structure of half-span $\phi^* = 0.4$ The corresponding normalized membrane force is displayed as a function of the transverse centerspan deflection, w_0, for various values of the loading parameter, $\hat{\lambda}$, in Fig. 3. Upon examination of that figure it may be seen that when the loading parameter is at its critical value the transverse deflection remains essentially fixed as the circumferential edge load is increased, until the membrane force achieves its critical value. At this point *bifurcation buckling* (in either direction) is indicated, and the deflection increases without bound, in the context of the mathematical model employed. In this sense, when preloaded with the load parameter at its critical value, the shell structure behaves in a manner similar to that of a flat plate subjected to in-plane edge loading. It may be seen from the figure that for all other values of the loading parameter, the load-deflection paths approach the critical load path asymptotically. We refer to this type of behavior as *asymptotic buckling*. The shell structure thus behaves as an edge loaded flat plate with an initial imperfection. It is important to note that the sense in which the structure deflects depends on whether the pre-load, $\hat{\lambda}$, is less than or greater than $\hat{\lambda}_{cr}$. Corresponding paths

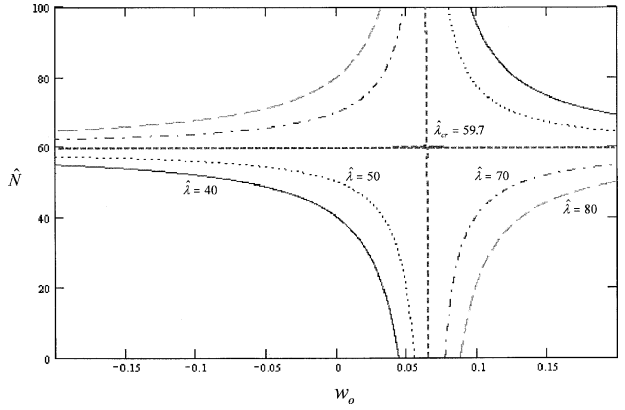

Fig. 3. Membrane force parameter versus transverse centerspan deflection for various values of the (transverse) loading parameter for a structure with clamped-free supports ($\phi^* = 0.4$).

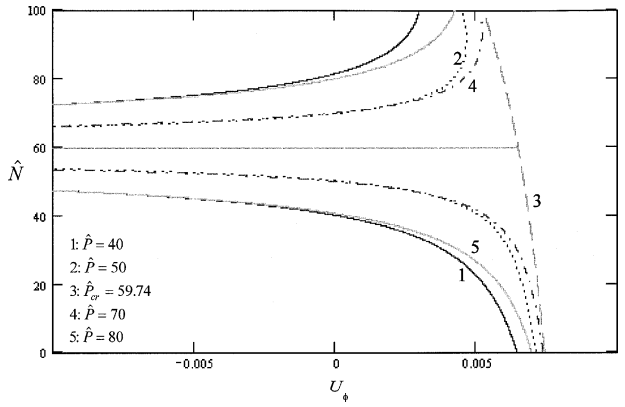

Fig. 4. Membrane force parameter versus circumferential edge deflection for various values of the applied pressure, with vanishing temperature change. Clamped-free supports ($\phi^* = 0.4$, $C^*/D^* = 2 \times 10^6$).

of the membrane force versus the circumferential edge deflection, U_ϕ, are displayed for various values of the loading parameter in Fig. 4, for a structure of the same span length and the specific stiffness ratio $C^*/D^* = 2 \times 10^6$, for the case of applied pressure and vanishing temperature change. Plots of the membrane force as a function of the transverse centerspan deflection for various span lengths are compared in Fig. 5, for $\hat{\lambda} = 50$. It is seen that structures of greater span length have a larger initial deflection due to the load parameter, and lower global stiffness, as would be expected. Parallel results for structures possessing the same material and geometric properties, but having pinned-free supports, are presented in Figs. 6–8 and show similar behavior.

6.2. Thermal loading

We next consider the behavior of multilayer shell segments which are fixed with regard to circumferential translation, and are subjected to a prescribed uniform temperature change only ($\hat{p} = 0$). Sample results are presented for the representative structures possessing the properties $\phi^* = 0.4$, $C^*/D^* = 2 \times 10^6$ and

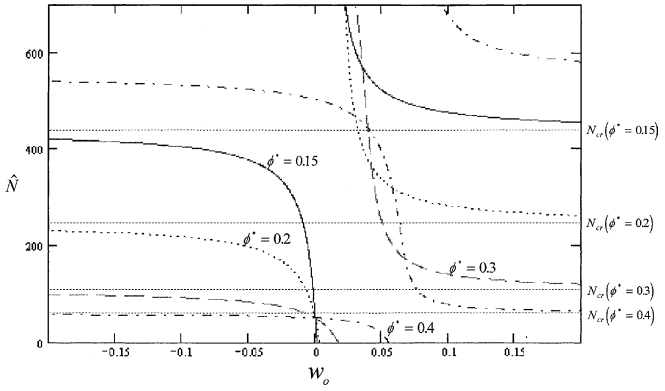

Fig. 5. Membrane force parameter versus transverse centerspan deflection for various (half) span lengths. Clamped-free supports ($\hat{\lambda} = 50$).

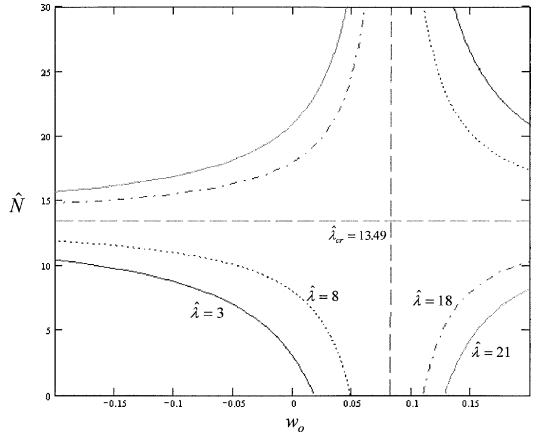

Fig. 6. Membrane force parameter versus transverse centerspan deflection for various values of the (transverse) loading parameter. Pinned-free supports ($\phi^* = 0.4$).

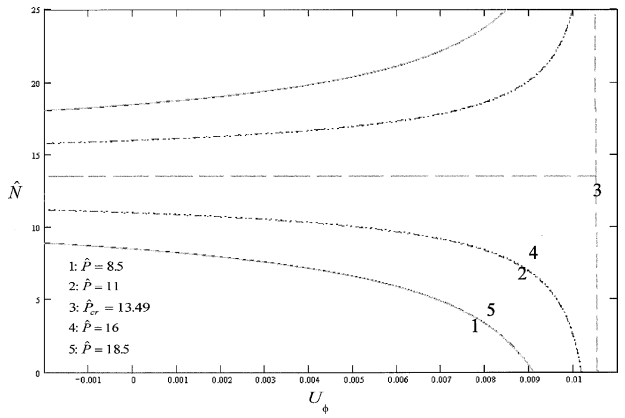

Fig. 7. Membrane force parameter versus circumferential edge deflection for various values of the applied pressure, with vanishing temperature change. Pinned-free supports ($\phi^* = 0.4$, $C^*/D^* = 2 \times 10^6$).

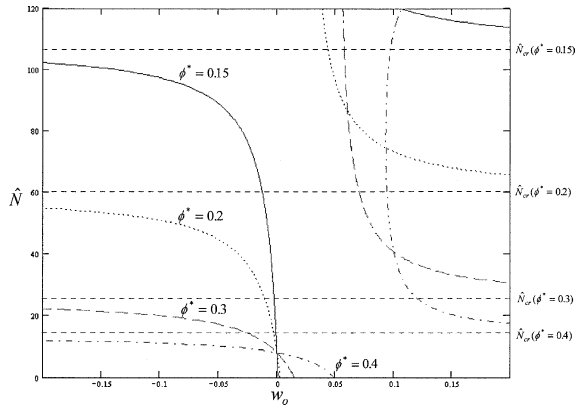

Fig. 8. Membrane force parameter versus transverse centerspan deflection for various (half) span lengths. Pinned-free supports ($\hat{\lambda} = 50$).

$n^*/m^* = 1 \times 10^3$, for both clamped-fixed and pinned-fixed support conditions. Plots of the roots of the integrability condition as a function of the prescribed normalized temperature change, for the case of clamped-fixed supports, are displayed in Fig. 9. It may be seen that multiple roots, and hence multiple equilibrium configurations, exist for a large range of values of the prescribed temperature change. In this regard, four branches of roots are identified in the figure, associated with the first four roots as they are encountered upon initial loading. [3] In that figure, point 'A' labels the point at which branches one and two cross. Thus, at this point, two equilibrium configurations exist for the same values of the temperature and membrane force. It may be noted that this point corresponds to $\widehat{N} = \widehat{N}_{cr}$ and $\hat{\lambda} = \hat{\lambda}_{cr} \leftrightarrow \widehat{\Theta} = \widehat{\Theta}_{cr}$ ($\hat{p} = 0$) defined by Eq. (17). It will be seen that this value of the thermal moment is associated with critical behavior of the structure. The corresponding plots of the stability function, F^*, are displayed in Fig. 10, and the

[3] It may be seen from Eq. (A.1), that the thermal moment, $\widehat{\Theta}$, increasing may imply either heating or cooling depending upon the sign of the material property m^*, as defined in Appendix C, for the particular structure of interest.

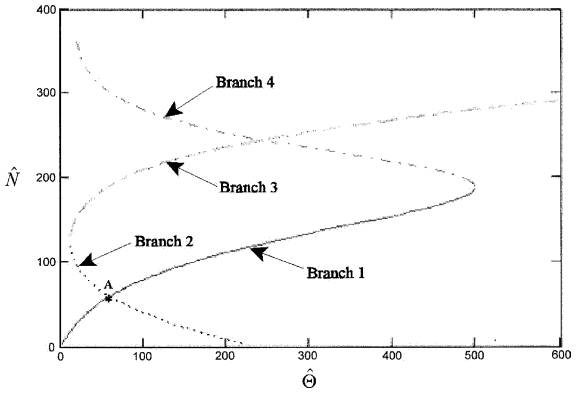

Fig. 9. Roots of integrability condition versus thermal moment. Clamped-fixed supports ($\phi^* = 0.4$, $C^*/D^* = 2 \times 10^6$, $n^*/m^* = 1 \times 10^3$).

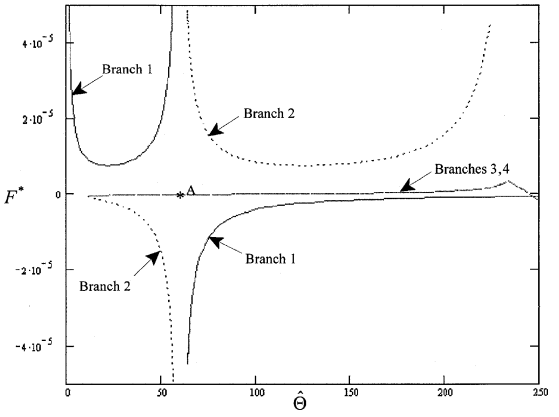

Fig. 10. Stability function versus membrane force parameter. Clamped-fixed supports ($\phi^* = 0.4$, $C^*/D^* = 2 \times 10^6$, $n^*/m^* = 1 \times 10^3$).

associated load-deflection paths expressed in the form of normalized temperature change (thermal moment), $\widehat{\Theta}$, versus normalized centerspan deflection, w_0, are displayed in Fig. 11. In each figure, the point(s) corresponding to the branch crossing in Fig. 9 is (are) labeled 'A'. As multiple equilibrium configurations exist for a given value of the thermal moment, we must assess which configurations are stable and which are not. Consideration of Fig. 10, together with the stability criterion established in Section 3, shows that the equilibrium configurations associated with the first branch of Fig. 9 are stable upon initial temperature change but become unstable when the level indicated by point 'A' is achieved. It may also be seen that the configurations associated with branch 2 are initially unstable, but become stable after the temperature change achieves the level indicated at point 'A'. [4] With this established, consideration of Fig. 11 shows that the structure initially deflects outward for increasing $\widehat{\Theta}$ until $\widehat{\Theta} = \widehat{\Theta}_{cr}$ (point 'A') at which point the structure "sling-shots" to a deflection in the opposite sense (i.e., inward), as indicated. We refer to this phenomenon as "sling-shot buckling" (Karlsson and Bottega, 2000a,c). [5] Further increases in the thermal

[4] Branches 3 and 4 actually lie slightly below $F^* = 0$, indicating that the associated equilibrium configurations are unstable, but are seen to become positive for large values of the temperature change.

[5] The phenomenon of sling-shot buckling was seen and named by Karlsson and Bottega (2000a,c) for patched structures under thermal loading. The mechanisms involved for that class of structures were similar to those of the present case.

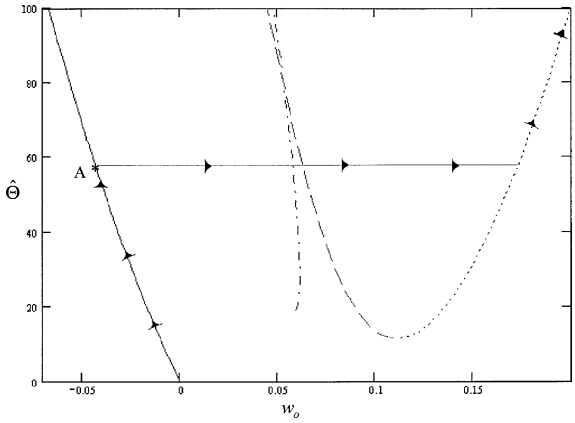

Fig. 11. Thermal moment versus centerspan deflection. Clamped-fixed supports ($\phi^* = 0.4$, $C^*/D^* = 2 \times 10^6$, $n^*/m^* = 1 \times 10^3$).

moment cause the structure to further deflect inwardly, as indicated. For the class of structures considered in the present study, this behavior is attributed to the fact that during the pre-buckling phase the amplitude of the deflection, $\widehat{Q}$, is dominated by the membrane force $\widehat{N}$, and hence the dominant motion is due to the overall thermal expansion of the structure. Once the critical temperature change is achieved, $\widehat{Q}$ is dominated by the thermal moment, $\widehat{\Theta}$, and thus the dominant motion is due to bending of the composite structure resulting from the disparity in thermal properties of the constituent layers. Parallel results for structures possessing the same material and geometric properties, but having pinned-free supports, are presented in Figs. 12–14 and show similar behavior.

6.3. Combined thermal and pressure loading

We next consider the influence of temperature change on the buckling behavior of pressure loaded layered panels, and vice-versa. It was shown recently by Rutgerson and Bottega (submitted for publication) for panels subjected to pressure loading alone, that snap-through buckling generally occurs well below the limit-load. We here examine how temperature change influences the behavior of pressure loaded shell

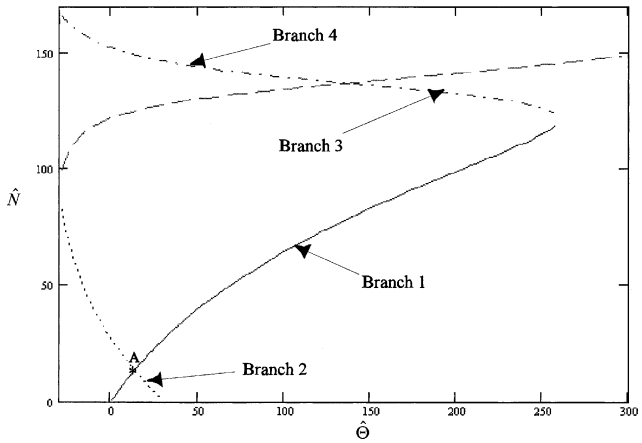

Fig. 12. Roots of integrability condition versus thermal moment. Pinned-fixed supports ($\phi^* = 0.4$, $C^*/D^* = 2 \times 10^6$, $n^*/m^* = 1 \times 10^3$).

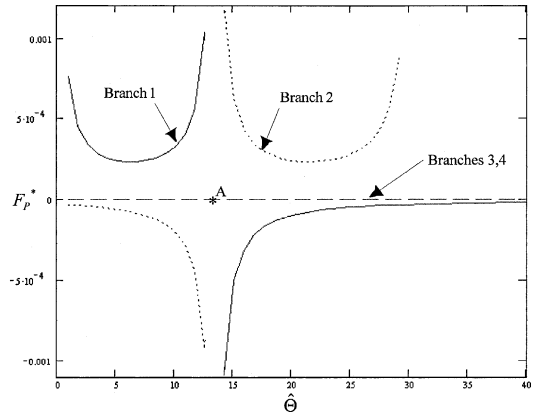

Fig. 13. Stability function versus membrane force parameter. Pinned-fixed supports ($\phi^* = 0.4$, $C^*/D^* = 2 \times 10^6$, $n^*/m^* = 1 \times 10^3$).

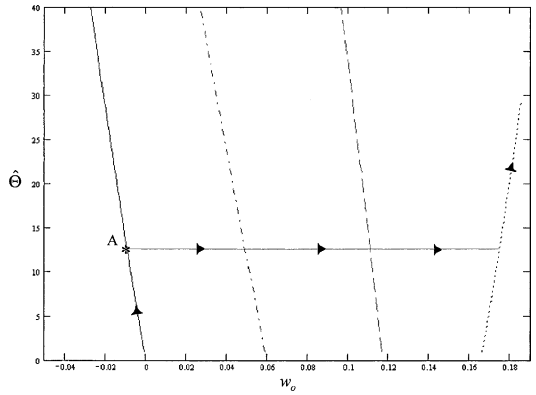

Fig. 14. Thermal moment versus centerspan deflection. Pinned-fixed supports ($\phi^* = 0.4$, $C^*/D^* = 2 \times 10^6$, $n^*/m^* = 1 \times 10^3$).

segments overall, and how it influences critical behavior in particular. Sample results are presented for representative structures possessing the properties $\phi^* = 0.4$, $C^*/D^* = 2 \times 10^6$ and $n^*/m^* = 1 \times 10^3$, for both clamped-fixed and pinned-fixed support conditions.

Plots of the roots of the integrability condition (4) as a function of the normalized applied pressure, $\hat{p}$, for various values of the renormalized temperature change (normalized thermal moment), $\widehat{\Theta}$, are displayed in Fig. 15 for the case of clamped-fixed supports. Branches corresponding to the first three roots of Eq. (4) are shown, and we again observe crossing of the first two branches as was seen for the case of thermal loading alone in Section 6.2, and for the case of pressure loading alone in (Rutgerson and Bottega, submitted for publication). In the figure, the branch crossing for each case is labeled 'A', and is associated with the critical value of the membrane force and the critical value of the loading parameter, as defined in Section 5. We define the corresponding value of the pressure at this point as the critical pressure, $\hat{p}_{\mathrm{cr}}$. A stability analysis using the criterion of Section 3 shows that the equilibrium configurations associated with the first branch are stable for pressures below this point and are unstable for pressures above this point. The reverse is found for the configurations associated with the second branch. The association of critical behavior with the crossing of the first two branches of the roots of the integrability condition was also seen for the thermally loaded structures considered in Section 6.2 and for the pressure loaded structures considered in

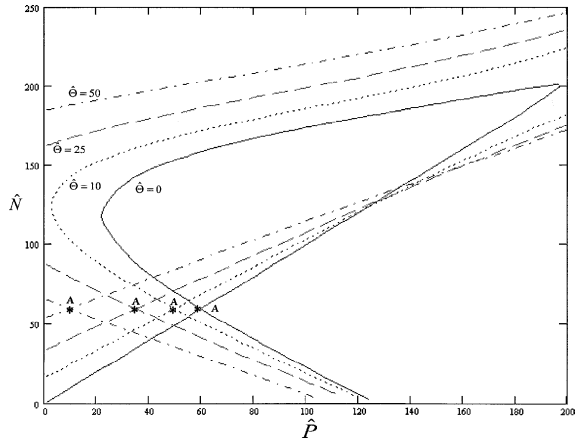

Fig. 15. Roots of the integrabilty condition as a function of the applied pressure for various values of the thermal moment. Clamped-fixed supports ($\phi^* = 0.4$, $C^*/D^* = 2 \times 10^6$, $n^*/m^* = 1 \times 10^3$).

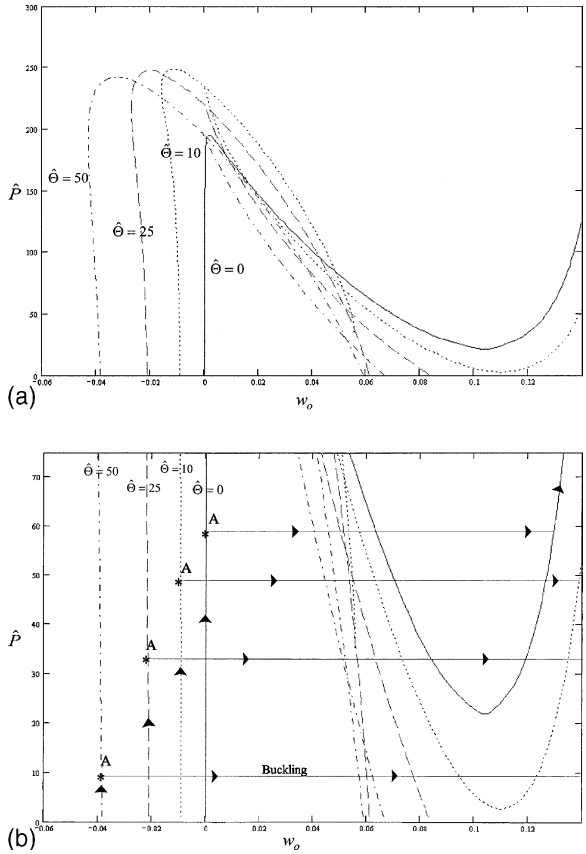

Fig. 16. Applied pressure versus transverse centerspan deflection for various values of the thermal moment. Clamped-fixed supports: (a) normal view, (b) localized view ($\phi^* = 0.4$, $C^*/D^* = 2 \times 10^6$, $n^*/m^* = 1 \times 10^3$).

(Rutgerson and Bottega, submitted for publication). It is seen, for the present case, that the critical pressure decreases as the temperature change is increased. This follows directly from the fact that the loading parameter is the sum of the pressure and thermal moment, as defined by Eq. (12), and that it is constant at this point (i.e., $\hat{\lambda} = \hat{\lambda}_{cr}$). The associated load-deflection curves, displayed in the form of the applied pressure versus the transverse centerspan deflection, are presented in Fig. 16(a) and (b). Fig. 16(a) shows that the temperature change bends the initial load path to the left, indicating that the structure initially deflects

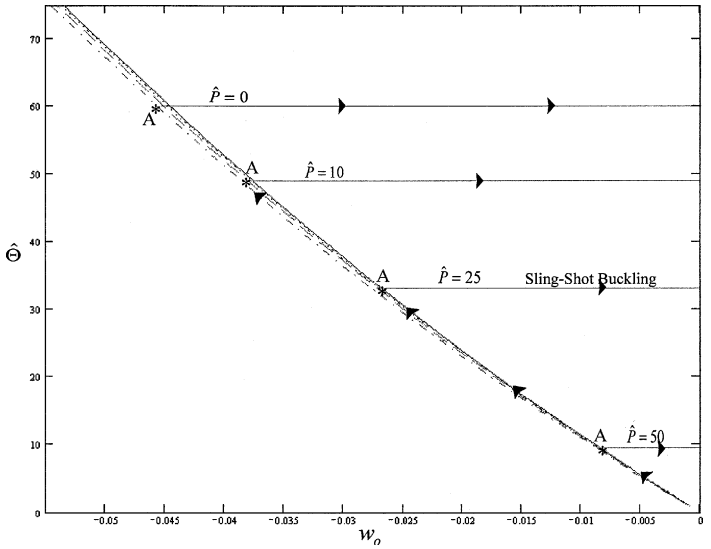

Fig. 17. Thermal moment versus centerspan deflection for various values of applied pressure. Clamped-fixed supports ($\phi^* = 0.4$, $C^*/D^* = 2 \times 10^6$, $n^*/m^* = 1 \times 10^3$).

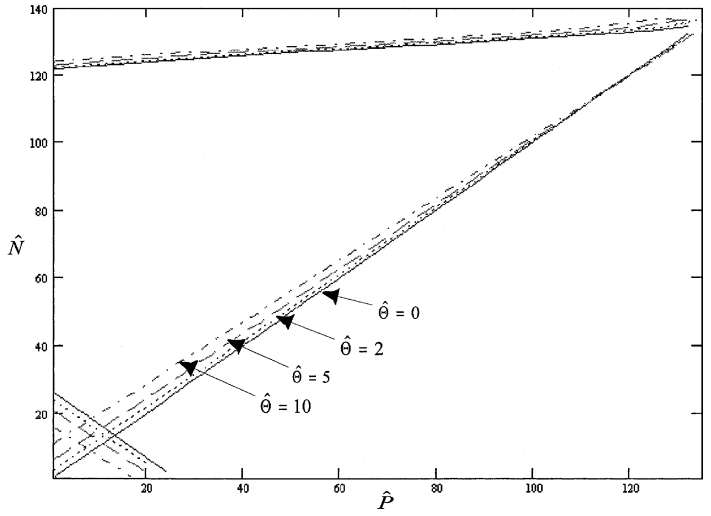

Fig. 18. Roots of the integrabilty condition as a function of the applied pressure for various values of the thermal moment. Pinned-fixed supports ($\phi^* = 0.4$, $C^*/D^* = 2 \times 10^6$, $n^*/m^* = 1 \times 10^3$).

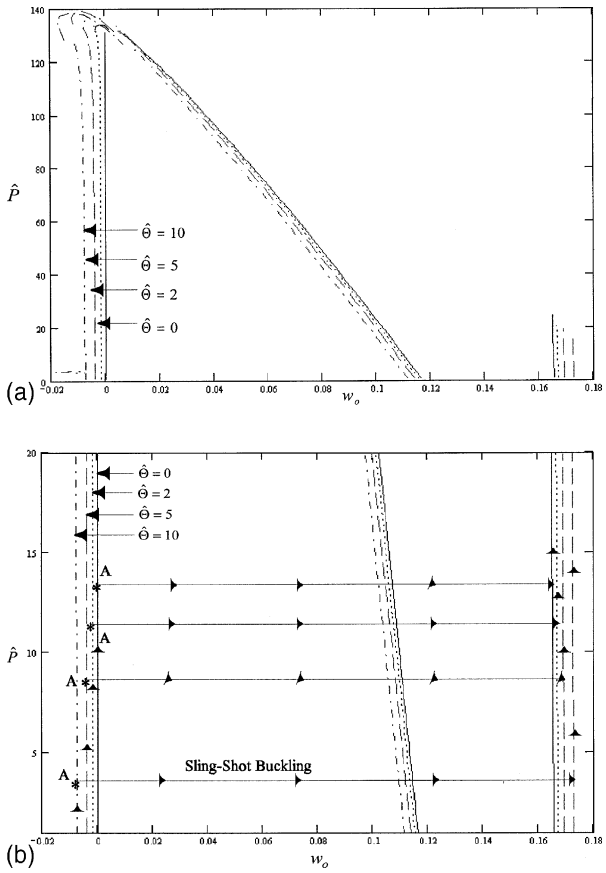

Fig. 19. Applied pressure versus transverse centerspan deflection for various values of the thermal moment. Pinned-fixed supports: (a) normal view, (b) localized view ($\phi^* = 0.4$, $C^*/D^* = 2 \times 10^6$, $n^*/m^* = 1 \times 10^3$).

outward as the temperature change is increased. It also shows that the pressure associated with the limit point is increased as the temperature change is increased. However, consideration of the localized view of these plots, displayed in Fig. 16(b), shows the critical point 'A', and hence the corresponding critical pressure for a given temperature. It is seen that buckling occurs at significantly lower values of the applied pressure than the limit point pressure and that this effect becomes more pronounced as the temperature change is increased. It is further seen that the "unstable well", and hence the "jump" in deflection during buckling, becomes larger with increasing temperature change. Finally, it is seen upon consideration of both Fig. 16(a) and (b) that where pre-limit point snap-through was indicated for vanishing temperature change, $\widehat{\Theta} = 0$ (Rutgerson and Bottega, submitted for publication), "sling-shot buckling" is indicated for non-vanishing temperature change, $\widehat{\Theta} > 0$. Thus, the effect of temperature change is to induce "sling-shot buckling", rather than "pre-limit snap through", at lower pressures and that the instability, as characterized by the jump in the transverse deflection, is rendered more severe.

A localized view of the load-deflection curves, in the form of normalized temperature change (thermal moment) versus the normalized centerspan deflection for various values of the applied pressure, for the identical structure are presented in Fig. 17 and demonstrate the complementary effects of pressure on the thermally loaded structure of Section 6.2. It is seen that the critical temperature is lowered, but that the corresponding load-deflection path is only slightly altered, by the presence of external pressure within

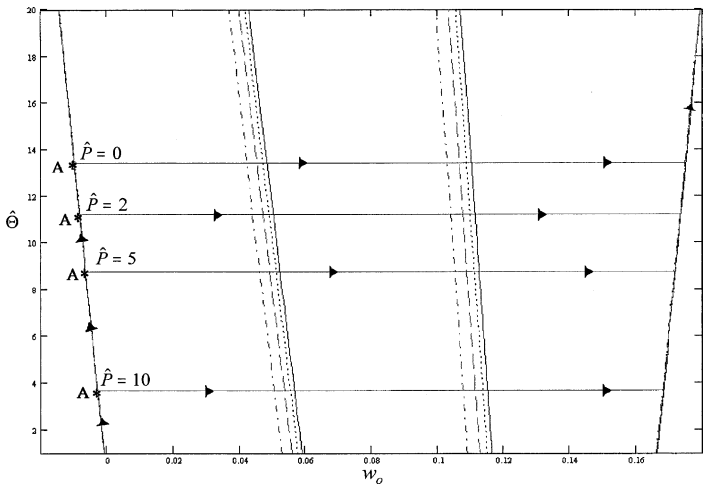

Fig. 20. Thermal moment versus centerspan deflection for various values of applied pressure. Pinned-fixed supports ($\phi^* = 0.4$, $C^*/D^* = 2 \times 10^6$, $n^*/m^* = 1 \times 10^3$).

the range of pressures considered. The effect is the same for temperatures outside the range shown, but the associated deflections are beyond the range of validity for the model employed.

Parallel results for structures possessing the same material and geometric properties, but having pinned-free supports, are presented in Figs. 18–20 and show similar behavior.

7. Concluding remarks

The behavior of multilayer shell segments has been studied for structures subjected to combinations of uniform temperature change, applied external pressure and applied and reactive compressive circumferential edge loads. The problem was expressed in a "mixed formulation", in terms of the normalized transverse (radial deflection) and a normalized membrane force parameter, and the structure is seen to be effectively defined by a ratio of composite mechanical stiffnesses, a ratio of composite thermo-mechanical stiffnesses and the normalized half span length. A stability criterion was established and a (transverse) loading parameter, consisting of the thermal moment (normalized temperature change) and normalized applied pressure, was identified. Critical parameters, consisting of a critical membrane force and critical (transverse) loading parameter were characterized as well, and were seen to be independent, and effectively independent, of the material properties of the system. Closed form analytical solutions of the corresponding non-linear problem were obtained and numerical simulations, based on these solutions, were performed.

For the case of applied circumferential edge loading (clamped-free and pinned-free supports), it was seen that the value of the transverse loading parameter governed the direction of the subsequent deflections. For structures that were preloaded with the transverse loading parameter at its critical value, the structure was seen to undergo effectively no subsequent transverse deflection beyond that due to the loading parameter alone, until the corresponding membrane force achieved its critical value as well. At this point bifurcation buckling was seen to occur, with the structure achieving large radial deflections in either direction. For structures preloaded with the loading parameter below (above) its critical value, the structure was seen to deflect in an outward (inward) sense from the initial deflection upon application of the circumferential edge load, and to exhibit "asymptotic buckling" in the same direction, as the corresponding membrane force approached its critical value.

For structures whose edges were fixed with regard to circumferential translation (clamped-fixed or pinned-fixed supports), critical behavior was seen to be associated with the crossing of the first two branches of the roots of the "integrability condition" for the circumferential displacements, indicating two possible equilibrium configurations at that point. The root crossing occurred when the transverse loading parameter and the membrane force parameter simultaneously achieved their critical values. A stability analysis showed that the equilibrium configurations associated with the first branch were stable upon loading, but became unstable when the loading parameter achieved its critical value. The reverse was seen for the equilibrium configurations associated with the second branch. For structures subjected to a temperature change alone, the structure was seen to initially deflect in an outward sense until the critical temperature change was achieved. At this point "sling-shot buckling" was seen to occur, where the structure violently "slings" from an outwardly deflected configuration to an inwardly deflected configuration. The structure is then seen to further deflect in an inward sense, in a stable manner, as the temperature change is further increased.

Instabilities associated with structures subjected to pressure loading were seen to become more severe when the effects of temperature change were included. Specifically, such structures were seen to exhibit pre-limit load snap-through buckling when no temperature change was present (Rutgerson and Bottega, submitted for publication). However, in the presence of temperature change, these same structures would first deflect outward with increasing pressure and then exhibit "sling-shot buckling" (rather than classic snap-through) when the critical pressure level was achieved. Further, the critical pressure levels at which buckling ensues were lowered as a result of the temperature change, and the decrease in critical pressure and the extent of buckling was seen to be continuously enhanced with increasing temperature change. Similarly, the critical temperature at which "sling-shot buckling" is initiated during temperature controlled loading was seen to be lowered by the presence of applied pressure, though the initial load-deflection path was seen to be only slightly altered by the applied pressure.

To close, critical non-linear behavior of multilayer shell segments subjected to combinations of uniform temperature change, external pressure and edge load has been elucidated, characterized, quantified and explained, and characteristic behavior has been demonstrated. Such structures are seen to exhibit a variety of interesting, and perhaps heretofore unanticipated, responses which can have significant ramifications.

Appendix A. Temperature scale

The renormalized temperature change (distributed thermal moment) is given by

$$\widehat{\boldsymbol{\Theta}} = \frac{m^*}{D^*}\widetilde{\boldsymbol{\Theta}}, \tag{A.1}$$

where the material parameters m^* and D^* are defined in Appendix C, and the normalized temperature change, $\widetilde{\boldsymbol{\Theta}}$, and hence the temperature scale for the class of problems of interest, is defined by

$$\widetilde{\boldsymbol{\Theta}} = \alpha_1\Theta = \alpha_1(\bar{\boldsymbol{\Theta}} - \bar{\boldsymbol{\Theta}}_0)/\bar{\boldsymbol{\Theta}}_0. \tag{A.2}$$

In Eq. (A.2), $\bar{\boldsymbol{\Theta}}$ is the dimensional temperature and $\bar{\boldsymbol{\Theta}}_0$ is the associated reference temperature. In addition, α_i $(i = 1, 2, \ldots, \Gamma)$ corresponds to the normalized coefficient of thermal expansion of layer 'i' of a structure comprised of Γ layers, where

$$\alpha_i = \bar{\alpha}_i\bar{\boldsymbol{\Theta}}_0(1 + qv_i) \quad (i = 1, 2, \ldots, \Gamma), \quad [q = 0 \text{ (plane stress)}, q = 1 \text{ (plane strain)}], \tag{A.3}$$

and $\bar{\alpha}_i$ $(i = 1, 2, \ldots, \Gamma)$ is the dimensional coefficient of thermal expansion of layer 'i'.

We further introduce the ratios

$$\alpha_i^0 = \alpha_i/\alpha_1 \quad (i = 1, 2, \ldots, \Gamma). \tag{A.4}$$

Appendix B. Deformation-displacement relations

The composite shell is considered as an assemblage of Γ individual shells (Bottega, 1994; Bottega and Karlsson, 1999; Karlsson and Bottega, 2000a). The membrane strain, $e^*(\theta)$, and the normalized curvature change, $\kappa(\theta)$, at the reference surface of the composite shell are given in terms of the corresponding normalized circumferential displacement, $u^*(\theta)$, and the normalized radial displacement, $w(\theta)$, by the relations

$$e^*(\theta) = u^{*\prime}(\theta) - w(\theta) + \tfrac{1}{2}w'^2(\theta), \tag{B.1a}$$

$$\kappa(\theta) = w''(\theta) + w(\theta). \tag{B.1b}$$

The circumferential displacement at the neutral axis of the composite structure, $\hat{u}(\theta)$, is related to its counterpart at the reference surface by the relation

$$\hat{u}(\theta) = u^*(\theta) + \rho^* w'(\theta), \tag{B.2}$$

where the material parameter ρ^* gives the location of the neutral surface of the composite structure with respect to the reference surface and is defined by Eq. (C.2e).

Appendix C. Constitutive relations

The normalized resultant membrane force, N^*, acting on the cross section of the composite structure, and the normalized resultant bending moment, M^*, acting about an axis through the reference surface of the composite structure, are expressed in terms of the membrane strain at the reference surface, e^*, the normalized curvature change, κ^* (see Appendix B), and the normalized temperature change, $\widetilde{\Theta}$ (see Appendix A), by the relations

$$N^*(\theta) = C^* e^*(\theta) + B^* \kappa^*(\theta) - n^* \widetilde{\Theta}, \tag{C.1a}$$

$$M^*(\theta) = A^* \kappa^*(\theta) + B^* e^*(\theta) - \mu^* \widetilde{\Theta} = D^* \kappa^*(\theta) + \rho^* N^*(\theta) - m^* \widetilde{\Theta}. \tag{C.1b}$$

The normalized composite stiffnesses appearing in Eqs. (C.1a) and (C.1b) are related to the normalized membrane and bending stiffnesses of layer 'i', C_i and D_i respectively, and the ratio of normalized coefficients of thermal expansion, α_i^0, by

$$A^* = \sum_{i=1}^{\Gamma} [D_i + \rho_i^2 C_i], \qquad B^* = \sum_{i=1}^{\Gamma} \rho_i C_i, \qquad C^* = \sum_{i=1}^{\Gamma} C_i, \tag{C.2a–c}$$

$$D^* = A^* - \rho^* B^*, \tag{C.2d}$$

$$\rho^* = B^*/C^*, \tag{C.2e}$$

$$n^* = \sum_{i=1}^{\Gamma} \alpha_i^0 C_i, \qquad \mu^* = \sum_{i=1}^{\Gamma} \alpha_i^0 \rho_i C_i, \qquad m^* = \mu^* - \rho^* n^*, \tag{C.3a–c}$$

where α_i^0 is defined by Eq. (A.4), and the normalized stiffnesses of the individual layers are defined below. In addition, the radial coordinate ρ_i (positive outward) locates the centroid of layer 'i' with respect to the reference surface.

The mechanical stiffnesses of the individual layers are normalized with respect to the bending stiffness of layer 1, and the dimensional radius of the undeformed reference surface. The explicit forms are given by

$$C_1 = 12/h_1^2, \qquad D_1 = 1, \tag{C.4a, b}$$

$$C_i = C_1 E_i^0 t_i, \qquad D_i = E_i^0 t_i^3 \qquad (i = 2, \ldots, \Gamma), \tag{C.4c, d}$$

where

$$t_i = h_i/h_1, \qquad E_i^0 = E_i/E_1 \qquad (i = 2, \ldots, \Gamma), \tag{C.5a, b}$$

$$E_i = \overline{E}_i \quad \text{(plane stress)} \quad \text{or} \quad E_i = \overline{E}_i/(1 - v_i^2) \quad \text{(plane strain)} \quad (i = 1, 2, \ldots, \Gamma). \tag{C.6a, b}$$

In Eq. (C.6a,b) the parameters $\overline{E}_i$ and v_i respectively correspond to the (dimensional) Young's modulus and Poisson's ratio for layer 'i'.

Appendix D. Normalization of loads

The renormalized pressure, $\hat{p}$, renormalized membrane force, $\widehat{N}$, and renormalized edge load, $\widehat{N}_\phi$, are defined in terms of their dimensional counterparts, $\bar{p}$, $\overline{N}^*$ and $\overline{N}_\phi$ by

$$\hat{p} = \frac{p}{D^*}, \qquad \widehat{N} = -\frac{N^*}{D^*}, \qquad \widehat{N}_\phi = -\frac{N_\phi}{D^*}, \tag{D.1a–c}$$

where

$$p = \frac{\bar{p}\overline{R}^2}{\overline{D}_1}, \qquad N^* = \frac{\overline{N}^*\overline{R}^2}{\overline{D}_1}, \qquad N_\phi = \frac{\overline{N}_\phi\overline{R}^2}{\overline{D}_1}, \tag{D.2a–c}$$

the non-dimensional stiffness D^* is defined by Eq. (C.2d), $\overline{R}$ is the dimensional radius of the reference surface and $\overline{D}_1$ is the dimensional bending stiffness of the innermost layer.

References

Boley, B.A., Weiner, J.H., 1960. Theory of Thermal Stresses. Wiley, New York, pp. 415–418.

Bottega, W.J., 1994. On circumferential splitting of a laminated cylindrical shell. Int. J. Solids Struct. 31, 1891–1909.

Bottega, W.J., Karlsson, A.M., 1999. On the detachment of step-tapered doublers: Part 1—Foundations. Int. J. Solids Struct. 36, 1597–1623.

Bottega W.J., Rutgerson, S.E., 2001. Thermo-mechanical instabilities in bilaminate shell structures. Symposium to Honor Professor G.J. Simitses, Contemporary Research in Engineering Mechanics, AD-65/AMD-249, Proceedings of the 2001 ASME International Congress, New York, November 2001, pp. 231–243.

Brevik, N.L., Hyer, M.W., 1998. Buckling and postbuckling of curved composite panels due to thermal and mechanical loading. J. Reinf. Plast. Compos. 17, 1298–1306.

Chen, L.W., Chen, L.Y., 1990. Thermal buckling analysis of laminated cylindrical plates by finite element method. Comput. Struct. 34, 71–78.

Gauss, R.C., Antman, S.S., 1984. Large thermal buckling of nonuniform beams and plates. Int. J. Solids Struct. 20, 979–1000.

Hamamoto, A., Hyer, M.W., 1987. Non-linear temperature-curvature relationships for unsymmetric graphite-epoxy laminates. Int. J. Solids Struct. 23, 919–935.

Huang, N.N., Tauchert, T.R., 1988. Postbuckling response of antisymmetric angle-ply laminates to uniform temperature loading. ACTA Mech. 72, 173–183.

Huang, N.N., Tauchert, T.R., 1991. Large deflections of laminated cylindrical and doubly-curved panels under thermal loading. Comput. Struct. 41, 303–312.

Karlsson, A.M., Bottega, W.J., 2000a. On thermal buckling of patched beam-plates. Int. J. Solids Struct. 37, 4655–4690.

Karlsson, A.M., Bottega, W.J., 2000b. On the behavior of a class of patched plates during cooling. Int. J. Non-Linear Mech. 35, 543–566.

Karlsson, A.M., Bottega, W.J., 2000c. Thermo-mechanical response of patched plates. AIAA J. 38, 1055–1062.

Librescu, L., Souza, M.A., 1993. Post-buckling of geometrically imperfect shear-deformable flat panels under combined thermal and compressive edge loadings. ASME J. Appl. Mech. 60, 526–533.

Mahayni, M.A., 1966. Thermal buckling of shallow shells. Int. J. Solids Struct. 2, 167–180.

Muller de Almeida, S.F., Hansen, J.S., 1997. Enhanced elastic buckling loads of composite plates with tailored thermal residual stresses. ASME J. Appl. Mech. 64, 772–780.

Noor, A.K., Burton, W.S., 1992. Computational models for high-temperature multilayered composite plates and shells. Appl. Mech. Rev. 45, 157–170.

Noor, A.K., Peters, J.M., 1992a. Postbuckling of multilayered composite plates subjected to combined axial and thermal loads. In: Thorton, E.A. (Ed.), Thermal Structures and Materials for High Speed Flight, AIAA Progress in Astronautics and Aeronautics 140, pp. 183–203.

Noor, A.K., Peters, J.M., 1992b. Thermomechanical buckling of multilayered composite plates. ASCE J. Eng. Mech. 118, 351–366.

Noor, A.K., Starns Jr., J.H., Peters, J.M., 1993. Thermomechanical buckling and postbuckling of multilayered composite panels. Compos. Struct. 23, 233–251.

Rutgerson, S.E., 2001. Nonlinear thermo-mechanical response of bilaminate composite shell structures. M.S. Thesis, Rutgers University, October 2001.

Rutgerson, S.E., Bottega, W.J., submitted for publication. Pre-limit point buckling of layered cylindrical panels under pressure.

Tauchert, T.R., 1991. Thermally induced flexure, buckling and vibration of plates. Appl. Mech. Rev. 44, 347–360.

Timoshenko, S.P., 1925. Bending and buckling of bimetallic strips. J. Opt. Soc. Amer. 11, 233–255.

Wahl, A.M., 1944. Analysis of the Valverde thermostat. ASME J. Appl. Mech. 11, A183–A189.

Wittrick, W.H., 1953. Stability of a bimetallic disk—Part I. Quart. J. Mechs. Appl. Math. 6, 15–26.

Wittrick, W.H., Myers, D.M., Blunden, W.R., 1953. Stability of a bimetallic disk—Part II. Quart. J. Mechs. Appl. Math. 6, 26–31.

Yin, W.L., 1998. Thermomechanical buckling of delaminated composite laminates. Int. J. Solids Struct. 35, 2639–2653.